OCEAN
ISSN 3008-1203

Open Access
Review Article

Synergizing machine learning with fluid–structure interaction research: An overview of trends and challenges

Muk Chen Ong✉ and Guang Yin

Department of Mechanical and Structural Engineering and Materials Science, University of Stavanger, Stavanger 4036, Norway

Cite This: *Ocean*, **2025**, *1*, 9470002

Read Online

ABSTRACT: Fluid–structure interaction (FSI) is a ubiquitous physical phenomenon in ocean engineering, which is critical in the design and operations of various marine structures and underwater vehicles. Especially, in a low-carbon society, FSI plays a pivotal role in the development of hydrokinetic energy conversion devices in ocean renewable energy. For FSI problems, strong nonlinear interactions between flow and structures, as well as turbulent flow pose significant challenges for understanding and predicting the dynamics of the FSI system. Facing these challenges and driven by the motivation of harnessing clean energy from ocean currents and waves, modern machine learning (ML) provides a novel and revolutionary solution to reduce the time and cost associated with traditional methodology in understanding the FSI physics, predicting the FSI dynamics and control for the engineering design. This paper focuses on the transformative potential of modern ML techniques in ocean engineering and presents a review of the current state-of-art ML applications in analyzing complex FSI phenomena within this field. Relevant ML algorithms and techniques are highlighted and the challenges of integrating these techniques into FSI problems are discussed.

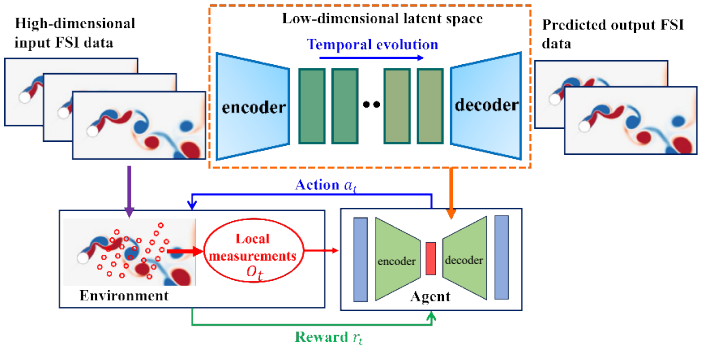

KEYWORDS: fluid–structure interaction (FSI), machine learning (ML), dynamics, prediction, control

1 Introduction

Fluid–structure interaction (FSI) phenomena can be observed everywhere in ocean engineering. The unsteady loadings generated from the interactions between the flows and the structures are crucial to determine the performance and safety of various marine structures such as rigs, subsea pipelines, power cables, ship propellers, autonomous underwater vehicles, and fish cages. Figure 1 shows some relevant examples. Especially, FSI is a critical problem in many leading renewable energy technologies such as wind, wave, and tidal energy conversion systems, where the core idea is to harness energy from flow-induced structural responses.

FSI involves a complex interaction between solid structures that are moving and deformed by the fluid flow and the surrounding fluid flow field influenced by the moving body. A brief outline of the interaction can be summarized as follows: The moving and deformed structures modify the boundary conditions for fluid flows, thereby altering the characteristics of the flow fields. In turn, these flows exert forces on the structures, arising from both pressure and viscous effects, which then drive the movements and deformations of the structures. This process, known as the structural response, creates a complex interplay between fluid dynamics and structural integrity in various spatial and temporal scales. The study of FSI systems is an important subject, especially for the safety and reliability design of marine structures. For example, the flow-induced flutter of highly flexible wind turbine blades strongly influences the stability and fatigue life of the blades and hence the safety of the whole wind turbine. The interaction between structures, wind, currents and waves should be considered during the installation operations of offshore wind turbines and subsea pipelines. Furthermore, understanding the FSI physics enables innovation and development of new renewable energy converters. For example, new varieties of ocean renewable energy devices have drawn inspiration from the movements of flapping or oscillating wings, following the discovery that flapping motion can transition from a mode of propulsion to one of energy extraction. This transition hinges on a precise phase relationship between the wing's pitch and heave [6–8]. The efficiency of the energy conversion depends on the surrounding flow influenced by the prescribed motion patterns and the shape of the wings. Gaining information on the hydrodynamic or aerodynamic loads on structures, structural motions and deformations as well as the

Received: April 6, 2024; **Revised:** May 5, 2024
Accepted: May 11, 2024

✉Address correspondence to Muk Chen Ong, E-mail: muk.c.ong@uis.no

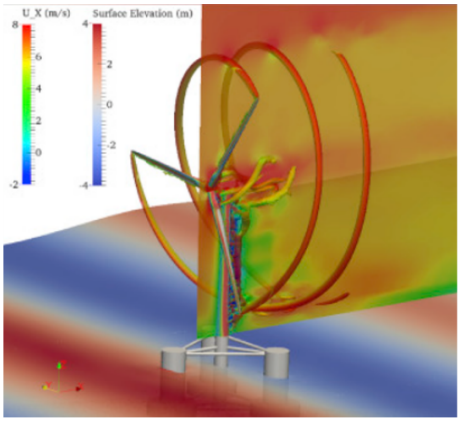

(a) Floating offshore wind turbine

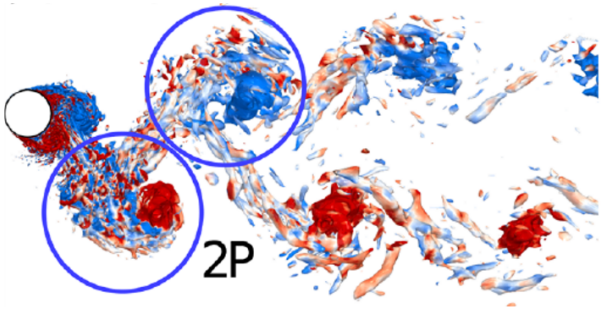

(b) FIV of a subsea pipeline

(d) Autonomous underwater vehicle

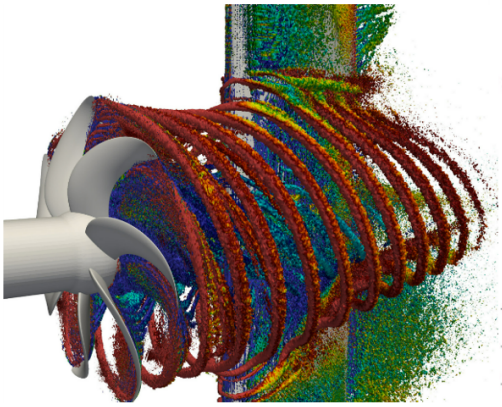

(c) Ship propellor with a downstream hydrofoil

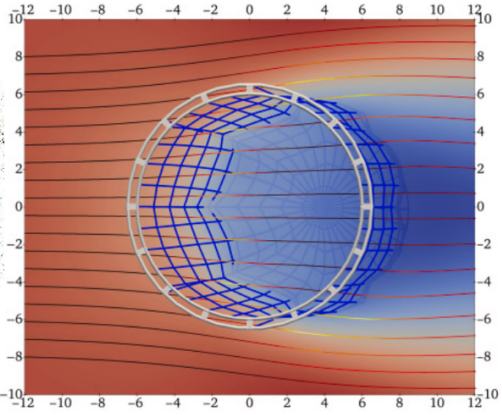

(e) Fish cage

Figure 1 Some examples of FSI systems in nature and engineering. (a) a fully coupled aero-hydro system of a floating offshore wind turbine. Adapted from Ref. [1] under the CC BY 4.0 license ©2017, The Authors. (b) A flow-induced vibrating subsea pipeline. Adapted from Ref. [2] with permission ©2024, AIP Publishing. (c) Ship propellor with a downstream hydrofoil. Adapted from Ref. [3] under the CC BY 4.0 license ©2023, The Authors. (d) Autonomous underwater vehicle. Adapted from Ref. [4] with permission ©2024, AIP Publishing. (e) Fish cage. Adapted from Ref. [5] under the CC BY 4.0 license ©2021, The Authors.

surrounding flow fields, is the primary objective of FSI research. From the industrial perspective, the dynamic response of engineering structures interacting with the fluid flow can be in practice detected only through limited measurements of the system. The implication of "non-intrusive sensing" is combined with our incomplete knowledge of the FSI system. This problem may lead to a fundamental misinterpretation of the underlying physics. For instance, measuring pointwise velocity signals in the wake flow behind a flow-induced-vibration (FIV) slender structure yields a sinuous time series that provides limited insight into the evolution of wake vortices, the movement of the structure, or the overall state of the FSI system.

This review paper aims to bridge these gaps by exploring the application of machine learning (ML) in FSI research. ML emerges as a promising solution for enhancing the physical understanding and dynamics prediction of FSI phenomena and potentially overcoming the constraints of conventional methodologies. The paper is organized as follows: First, an overview of traditional numerical simulation methodologies for studying FSI is provided; then, current knowledge of ML techniques within the field in terms of feature detection and dynamics prediction and control is highlighted; finally, both the challenges and opportunities are addressed.

2 Traditional approaches of investigating FSI

FSI problems have long been explored through experimental studies. However, the advancement of numerical models has enhanced the ability to comprehensively understand flow patterns and structural responses beyond experimental limitations. Generally, the numerical models of FSI fall into two primary categories: monolithic and partitioned approaches. The monolithic approach integrates both the fluid and structural dynamics into a single mathematical framework, creating one global system of nonlinear equations for the entire FSI problem. The system is then solved through a unified algorithm, which employs an implicit method for handling the conditions at the interface. On the other hand, the partitioned approach distinguishes the fluid and the structure into two computational domains, each utilizing distinct discretization techniques and solvers. This approach relies on

explicit treatments for the interfacial conditions to communicate information between the fluid and structural solvers. For the discretization of the governing equations, conforming or body-fitted mesh methods and non-conforming mesh methods are usually employed. The conforming mesh is moving and deforming in sync with the structural boundaries and treats the interface conditions between the structures and fluids as physical boundary conditions. During the simulation, the mesh is dynamically updated at every time step. Arbitrary Lagrangian–Eulerian (ALE) algorithms usually adopt the conforming mesh. The non-conforming mesh methods, associated with immerse boundary methods (IBMs), usually treat the interface conditions as constraints imposed on the governing equations of fluids and structures.

The advanced capabilities of modern supercomputers facilitate high-fidelity numerical simulations of FSI problems, encompassing complex three-dimensional (3D) turbulent flows and intricately coupled structural dynamics. The simulations offer detailed insight into the 3D flow phenomena, such as shear-layer separation, fluctuations in hydrodynamic or aerodynamic forces, and noise generations, thereby improving engineering design. Most engineering FSI problems are subject to turbulent flows characterized by spatial and temporal multi-scale features. The spatial scales can vary from the macroscopic scales of the structural dimensions (e.g., the diameter of pipelines, the chord length of wings and the length of a wind turbine blade) down to the microscopic Kolmogorov length scales, which represent the smallest scale of turbulence, associated with the Reynolds number. The Navier–Stokes (NS) equations governing the fluid flow can be solved by discretizing the equations into a high-dimensional dynamic system. It is well-known that the number of degrees of freedom of the governing equations is proportional to $Re^{37/14}$ [9], indicating a significantly large discretized system at high Re. Furthermore, the structures immersed in the fluid may undergo complicated flow-induced motions and deformations, which require solving their structural governing equations. Therefore, for an FSI problem, a coupling between a fluid and a structural solver is usually required, and the computational cost for solving the coupled system can easily exceed 10,000 CPU h [10] even for a single fluid and structural configuration. While parallel computing capabilities of supercomputers allow for such simulations, the process remains costly, with substantial memory requirements for data storage. These challenges impose limitations on the widespread application of numerical models for solving real-world engineering issues and for use in industrial settings.

3 ML as a novel approach

Nowadays, modern ML techniques allow for revolutionary changes towards system identifications and dynamic systems predictions across the fields of science and engineering. As a branch of artificial intelligence, ML can generally refer to the techniques to learn relationships among inputs and outputs from huge amounts of observation data and experimental data without explicit knowledge of the underlying physical law.

Mendez et al. [11] outlined the applications of ML in scientific and engineering problems outlined into five major stages: (1) problems, hypotheses or objectives definition; (2) collecting data for training through experiments, simulations or observation; (3) building the architectures of the model; (4) defining loss functions to be minimized; and finally; (5) selecting an optimization algorithm to update the parameters in the architectures of the model to achieve the minimization of the loss functions. ML methodologies are broadly classified into supervised, unsupervised, and semi-supervised techniques. Examples of relevant algorithms are shown in Fig. 2.

Supervised learning aims to learn a function mapping the training data to the labels. Classic supervised learning applications which involve discrete labels include the classification of images. Support vector machines (SVMs) [12], random forests [13] and *k*-nearest neighbours (KNN) [14] are the several most widely employed algorithm for classification. When it comes to the applications of FSI, supervised learning is used in flow regime identification. For example, gas–liquid two-phase flow is commonly observed in piping systems. Due to different gas–liquid superficial velocities, various flow forms such as stratified flow, wave flow, slug flow and annular flow are shown in the pipe flows. Understanding the multiphase flow and its influences on the structural responses of the pipes and monitoring and control of the two-phase flow process requires accurate identifications of the flow patterns. Supervised learning provides a novel approach to flow pattern identifications based on various flow measurement quantities such as pressure signals [15] or electrical capacitance tomography images of the flow [16]. For continuous labels, regression methods are used, which approximate a function using linear or quadratic curves to fit the continuous output data. There has been special interest in using regression algorithms in turbulence modelling as reported in works by Duraisamy et al. [17] and Tracy et al. [18], and optimal problems such as vehicle aeroacoustics improvement [19] and aerodynamic shape optimization [20].

Neural networks (NNs), inspired by biological NNs, are the most successful and well-known supervised learning. For a typical classification task, the central idea of the NN is mapping the input data (the input layer in the NN) to the label data (the output layer in the NN) through a series of cell layers (the hidden layer in the NN). An example of the NN architecture is shown in Fig. 3. Each cell refers to a neuron, which receives weighted input signals from multiple neurons in the upstream layer and generates an output signal, which is transferred to the downstream layer. Different numbers of neurons can be used to form each layer and different numbers of layers can be built. The connections between the adjacent layers can be all-to-all (fully connected layer) or partial. In addition, the mapping between layers can be nonlinear if nonlinear activation functions are used in each cell. Different types of nonlinear activation functions enable the flexibility of the NN. The training of NNs involves the backpropagation algorithms to

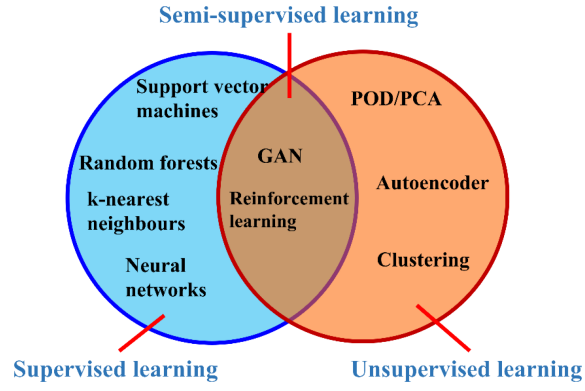

Figure 2 Some typical ML algorithms (PCA: principal component analysis).

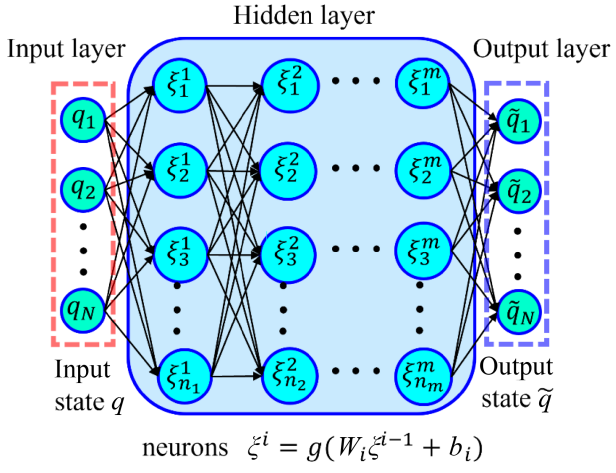

Figure 3 An example of FCN. The hidden layer consists of m cell layers and there are n_i neurons in i^{th} cell layer. Weights vector W_i and a nonlinear function g are used in each cell.

iteratively adjust the weights of the NN to minimize the error between the predicted output layer and labelled training data.

4 Applications of ML in FSI

The applications of ML in FSI research can be generally classified into three categories: feature detections and dynamics predictions and control, which will be introduced in this section. The recent advances of employing physics-informed NNs in FSI investigations will be also discussed.

4.1 Feature detections of FSI

The primary goal of feature detection for FSI systems is to obtain the low-dimensional manifold of the experimental data and simulations results. The low-dimensional manifold, also known as "modes" or "latent space", encapsulates dominant flow characteristics of the underlying FSI systems. There have been many modal decomposition techniques available in the fluid mechanics community. A typical example is the cylinder wake flow, which displays distinct shedding vortices allowing for a low-dimensional representation. For modal decomposition analysis, a variety of data including space- and time-resolved flow velocities, pressures and rigid structural velocities and displacements are commonly utilized for analysis.

Modal decomposition methods fall into two main categories based on their approach to learn these modes. The first one, a data-driven approach, obtains modes directly through postprocessing computational fluid dynamics (CFD) simulations and experimental data, analogous to the data training processes in ML. Both linear and nonlinear modal decomposition methods have been employed. Proper orthogonal decomposition (POD) and their modifications (such as spectral POD (SPOD) and multiresolution POD) belong to the linear methods. When utilizing the POD to analyze the flow field data, the resulting POD modes contain the fluid and structural motions that contribute most to the total energy of the FSI system. Since its introduction by Lumley [21], the POD technique has been widely adopted to analyze the bluff body flows. Relevant studies can be found in reports by Ilak et al. [22], Podvin et al. [23], Podvin [24], and Rowley et al. [25]. For applications of modal decompositions on FSI problems, special treatments must be designed to tackle the moving structure since classic POD analysis

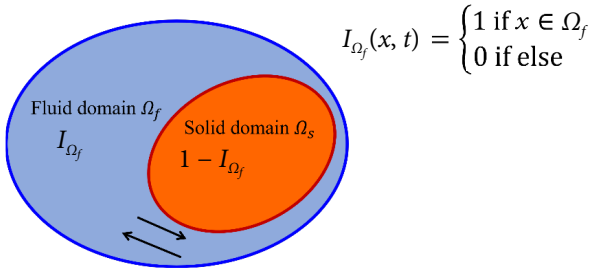

Figure 4 A schematic description of the variable $I_{\Omega_f}(x,t)$. Adapted from [26] with permission ©2010, Elsevier Ltd.

typically deals with flow data on stationary grids. Liberge et al. [26] proposed the method for a moving solid body by considering a fixed uniform grid containing the time-variant domain for both fluid and solid, and then introduce a global velocity field $\boldsymbol{u} = (1 - I_{\Omega_f})\boldsymbol{u}_s + I_{\Omega_f}\boldsymbol{u}_f$ with an additional variable $I_{\Omega_f}(x,t)$ as a function of the coordinate x and the time t to differentiate between the solid and fluid domains as shown in Fig. 4. Therefore, the POD modes are computed for the global velocity field $\boldsymbol{u}$. Riches et al. [27] used the POD method to analyze the experimental planar PIV data in the wake region behind a vibrating cylinder while excluding the moving cylinder itself from the analysis.

SPOD, developed by Towne et al. [28], Schmidt et al. [29], Schmidt et al. [30] and later adopted by Nidhan et al. [31] to study turbulent stratified wakes of a disks, was conducted in the frequency domain and can extract modes with monochromatic frequency content from statistically stationary flows. The multiscale POD (mPOD), proposed by Mendez et al. [32], introduces spectral constraints to the energy optimality of the POD modes obtained from the eigenvalue analysis of the correlation matrix of the flow field snapshots. The correlation matrix is first separated into contributions of different scales using the multiscale resolution analysis (MRA). Then, the POD is performed for each separate scale. Since the wake flow behind a vibrating cylinder displays a broad spectrum of spatiotemporal scales and unsteady transient behaviors, it is difficult to describe the FSI system by classic harmonic decomposition methods, such as the fast Fourier transform (FFT). Instead, the properties of mPOD make it exceptionally suitable for extracting coherent flow motions with non-overlapping portions of the frequency spectra of the chaotic wake flow. It still preserves the mutual orthogonality of the modes and ensures a good convergence with a finite number of dominant modes to represent the entire flow characteristics. In Janocha et al. [2], 3D mPOD was employed to study the wake flow of an FIV cylinder at three representative reduced velocities corresponding to the initial, upper and lower branches of vortex-induced vibration (VIV). The dominant flow features associated with the vortex shedding and their super harmonics and the 3D low-frequency modulation of the wake flow together with their frequency information were captured by the mPOD analysis.

Dynamic mode decomposition (DMD) and its modifications (such as multiresolution DMD and sparsity-promoting DMD) become increasingly popular since it was proposed by Schmid [33] for analyzing experimental and simulation flow data. Different from POD modes which represent the most energetic flow features, the resulting DMD modes are characterized by their unique oscillation frequencies and growth/decay rates, which emphasize the dynamics of each mode. The DMD modes are not orthogonal and this non-orthogonality poses challenges in evaluating the contribution and

dominance of these modes in the FSI system since the modes with very high amplitudes may be damped quickly during their temporal evolutions. An improved criterion for selecting dominant DMD modes was proposed by Kou et al. [34] and Kou et al. [35], which ordered each DMD mode by time integration of its time coefficient. A sparsity-promoting DMD algorithm was introduced by Jovanović et al. [36]. The algorithm uses optimization to achieve the least difference between the mode's combination and the matrix of snapshots and simultaneously achieve a desirable balance between the quality of the approximation and the number of modes required to approximate the training data. Moreover, for more complicated turbulent flow, high-order DMD was proposed by Le Clainche et al. [37] by considering time-lagged snapshots, which allowed to exploit the temporal redundancies.

Since the DMD analysis has its superiority in selecting dominant flow patterns associated with characteristic frequencies, it becomes a good tool for investigating the unsteady and transient properties of FSI systems. The characteristic vortex shedding frequencies and their harmonics were identified by DMD modes for two couple cylinders undergoing FIV by Janocha et al. [2]. The most energetic and the most dynamically important mode associated with the fundamental shedding frequency for single-cylinder configurations was identified. For the piggyback configuration of the two cylinders which was commonly observed in submarine pipelines to transport oil and gas between offshore and onshore production facilities, the gap flow between the two cylinders was found to be a dominant flow feature captured by the leading DMD modes. Also, it was observed that for the FIV cylinder cases, a significantly increasing number of DMD modes were necessary to achieve a low-dimensional representation of the FSI system at the given level of accuracy compared to the stationary cylinder configurations. Furthermore, the hydrodynamic forces acting on the cylinders, which are important quantities for engineering, are estimated using the dominant DMD modes combined with a force partitioning method (FPM) [38–40] by Yin et al. [41]. The contributions of dominant DMD modes to the drag and lift coefficients on the FIV cylinders were identified.

Moving beyond the conventional linear modal decomposition techniques, ML techniques are utilized to search for a nonlinear subspace of the original high-dimensional data. A NN-based autoencoder shows promising performance in learning a map from the high-dimensional state variable q to a low-dimensional latent-space representation of z which is called the encoder as $z = E(q)$, and the map, called decoder, back from the latent state to the predicted $\tilde{q}$ of the original high dimension as $\tilde{q} = D(z)$. The architecture autoencoder is trained to minimize the loss function between q and $\tilde{q}$ based on training data either from simulations or experiments. For deep learning, the encoder and the decoder can be composed of multiple layers of neurons (multilayer perceptrons (MLPs)), as shown in Fig. 5, which are called deep NNs (DNNs). Each node in these layers employs nonlinear activation functions to significantly compress useful information into a nonlinear low-dimensional latent space. Apart from MLPs, convolutional NNs (CNNs) [42] commonly employed for image processing can be also used to build the encoder and the decoder. A general schematic architecture of an encoder based on CNN is displayed in Fig. 6. CNNs employ a hierarchical structure of layer and each layer of a CNN mainly consists of three sub-layers: the convolutional layer, pooling layer and upsampling layer. For the convolutional layer, a filter h called kernel with a size of $H \times H \times K$ is scanning on the input signal z_{ijk}^{l-1} at the pixel of the input data from the upstream layer and this operation can be generally expressed as

$$z_{ijk}^{l} = \varphi\left(b_k^l + \sum_{m=0}^{K-1}\sum_{p=0}^{H-1}\sum_{s=0}^{H-1} h_{m,ps}^{l-1} z_{i+p-C,j+s-C,k}^{l-1}\right) \tag{1}$$

In this expression, z^{l-1} and z^{l} are the input and output variables of each layer, h^l (with components $h_{m,ps}^l$) and b^l (with components b_k^l) are the weights and the biases of the layer l, and φ is the activation function of each layer, enhancing the ability of the model to capture nonlinear characteristics in the system. Furthermore, the pooling operation compresses the data z^l by using an additional filter with a size of $P \times P$ to reduce dimensions. The pooling operation can take the maximum value (max-pooling) of the region of z^l scanned by the pooling operator or the averaged value (average-pooling) of the scanned region by the pooling operator. Therefore, the computational costs are reduced by a factor of $(1/P)^2$. Then, the upsampling operation is used to expand the data dimension by copying, nearest-neighbor or bilinear interpolation. The weights of CNN are obtained through optimizations on the

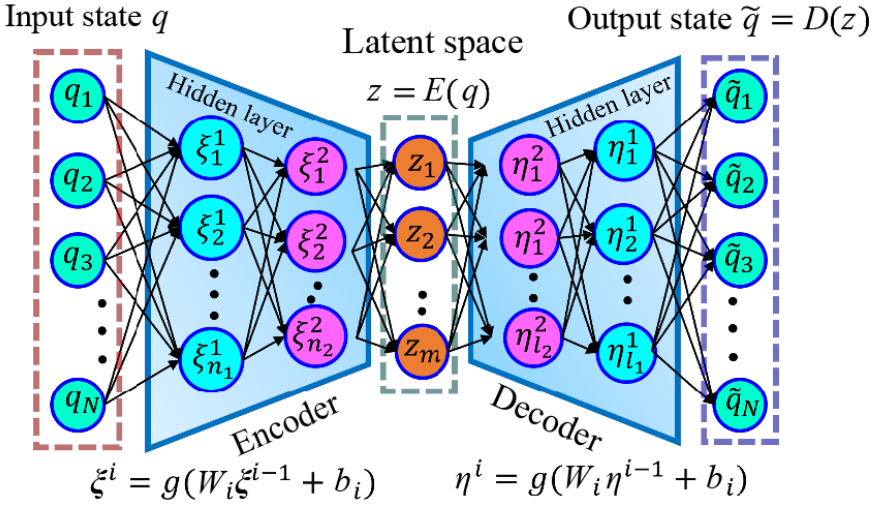

Figure 5 A schematic view of an autoencoder based on MLPs.

training data.

Murata et al. [43] and Fukami et al. [44] developed a modal decomposition method based on CNN combined autoencoder and applied it to a flow around a circular cylinder at $Re = 100$. A latent space with a dimension of $r = 2$ is obtained. Compared with the conventional POD method, a lower reconstruction error is achieved by using the nonlinear hyperbolic tangent activation function. Due to the nonlinear activation functions, CNN is suitable for processing the highly nonlinear and multiscale turbulence. Combined with POD, a fully-connected CNN (FCN) was built by Guastoni et al. [45] and used to predict the turbulence fluctuation and reconstruct the turbulent flow based on wall quantities in channel flows. The developed FCN-POD model exhibits superior performance in predicting the nonlinear interactions of the multiscale flow, the instantaneous fluctuation fields, the turbulence statistics and the power-spectral densities compared with the POD analysis. Other architectures such as generative-adversarial-network (GAN)-based models are used to reconstruct 3D turbulent flows from two-dimensional (2D) measurements by Yousif et al. [46]. Super-resolution GANs (SRGANs) were also applied to enhance the resolution of wall fields and predict the velocity fields at wall-parallel planes from coarse wall measurements in Güemes et al. [47].

More recently, variational autoencoders (VAEs), probabilistic models based on the variational Bayesian [48], have been developed to increase the efficiency of encoding the information of high-dimensional data. The resulting latent space is a probability distribution rather than a fixed point, therefore enabling the flexibility and continuity of the DNNs to generate new high-dimensional data, as shown in Fig. 6. Furthermore, a modified β-VAE variant developed by Higgins et al. [49] introduces a regularization parameter β in the loss function to improve the balance between the reconstruction accuracy of the latent space and the orthogonality of the latent space. As a result, more disentangled and interpretable representations are obtained. By applying the CNN-β-VAE model on the turbulent wake flow of a simplified urban environment, Eivazi et al. [50] showed that near-orthogonal latent space with a dimension of $r = 5$ could reconstruct the complex turbulent wake flow behind wall-mounted structures.

4.2 Dynamics predictions of FSI

Once the low-dimensional latent space of the FSI system is built, the next question is predicting the temporal evolution of the latent space and then reconstructing the future state of the system. For instance, as shown by the low-dimensional representation of Eq. (2) using the linear modal decomposition, if the temporal coefficient of each mode $a_i(t)$ $(0 \leqslant i \leqslant r)$ are known, the state of the FSI system at any given time can be reconstructed. Further quantities such as the loads imposed by the flows on the structures and the induced structural responses can be predicted from the reconstructed state. Again, compared with CFD simulations involving the integration of high-dimensional dynamic systems, the number of unknowns $a_i(t)$, r, is far fewer than the original number of degrees of freedom, and the dimension in solving the FSI systems is highly reduced, which results in the term "reduced-order models" (ROMs).

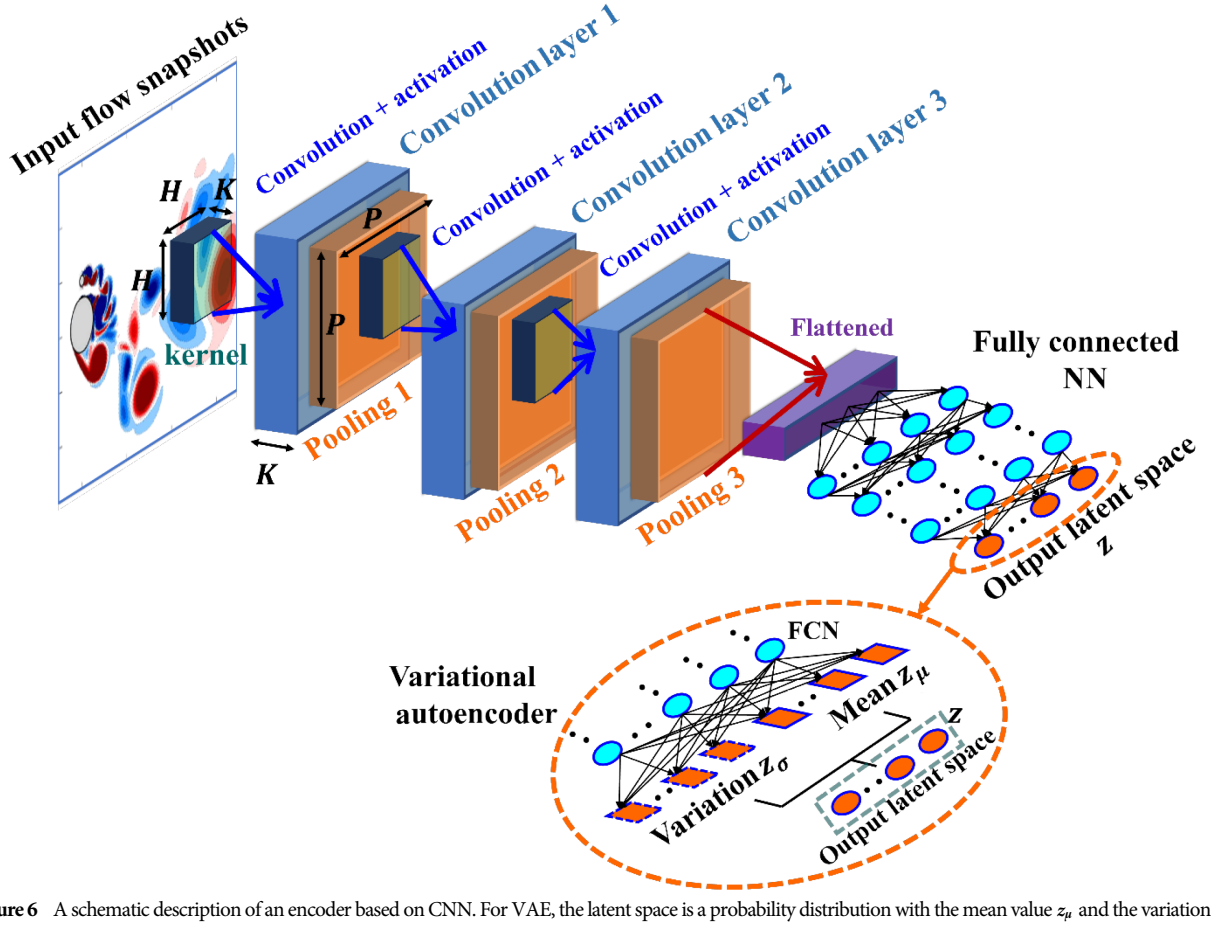

Figure 6 A schematic description of an encoder based on CNN. For VAE, the latent space is a probability distribution with the mean value z_μ and the variation z_σ.

https://doi.org/10.26599/OCEAN.2025.9470002

The present ROMs can be generally divided into two categories: a projection-based model and a data-driven model. The projection-based model, also known as intrusive ROM, usually adopts Galerkin projection, which orthogonally projects the governing partial differential equations (PDEs) of the FSI system onto the subspace spanned by the spatial modes set Φ using a projection operator $P = \Phi\left(\Phi^{\mathrm{T}}\Phi\right)^{-1}\Phi^{\mathrm{T}}$, where T denotes the transpose operation. If the modes are orthonormal such as POD modes, the projection operator is $P = \Phi\Phi^{\mathrm{T}}$. Then, a low-dimensional and simplified system of $\boldsymbol{a}(t) = [a_1(t), a_2(t), \ldots, a_r(t)]^{\mathrm{T}}$ can be obtained as

$$\frac{\mathrm{d}\boldsymbol{a}(t)}{\mathrm{d}t} = \widetilde{f}(\boldsymbol{a}(t)) \tag{2}$$

where the number of degrees of freedom is reduced to r (with $r \ll N$). This method has been successfully applied over decades for various flow problems, including Podvin et al. [23] and Podvin [24] for turbulent channel flows, Rowley [51] for compressible flows, Liberge et al. [26] for flows past an oscillatory cylinder, Östh et al. [52], Podvin et al. [53], and Podvin et al. [54,55] for flow over an Ahmed body. There are several modifications and optimizations for the POD mode-based ROM including the balanced POD (BPOD), which balances the controllability and observability of control problems of flow systems as used in Dadfar et al. [56] for attenuating the amplitude of the Tollmien-Schlichting (TS) waves inside the boundary layer of an airfoil and for linearized channel flow [51].

The data-driven models, also known as non-intrusive ROMs, are usually adopted when governing equations of the dynamical systems are unknown prior, especially in the fields where physical laws or the first principles remain unknown, such as neuroscience, climate sciences, biomedical engineering, and epidemiology. In data-driven models, the dynamics of the modes are identified directly from the measurement data. The DMD analysis belongs to this method. According to Schmid [33] and Bagheri [57], DMD is an approximation of the Koopman operator K_t of dynamical systems. The Koopman operator is an infinite-dimensional linear operator that acts on the measurement function g of the flow fields to predict the future state as $K_t g(q) = g(F^t(q))$, where $\boldsymbol{F}^t$ is defined as the time-forward map $F^t(q) = q + \int_0^t f(q)\,\mathrm{d}t'$, which is determined by the dynamical system. The measurement function g can then be linearly approximated by the eigenfunctions $\varphi_\lambda(q)$ of the operator along with their exponential time dependence λ, which satisfies the eigenrelations of $K_t\varphi_\lambda(q) = \varphi_\lambda(q)\exp(\lambda t)$. Finally, a low-dimensional representation of the flow state measurement at t can be expressed as $g(q(x,t)) \approx \sum_{n=1}^{N}\exp(\lambda_n t)\,\varphi_{\lambda_n}(q(x,0))\,\psi_n$, where ψ_n is denoted as Koopman modes. According to Sharma et al. [58], the DMD can be used to obtain the triple sequences $\{\varphi_{\lambda_n}, \psi_n, \lambda_n\}_{n=1}^{N}$ and dynamics of the system.

Nevertheless, the DMD method is still faced with challenges brought by strongly nonlinear dynamic system. Recently, sparse identification of nonlinear dynamics (SINDy) has been developed by to overcome the challenges of dealing with the strong nonlinearity of dynamical systems. In the framework of the SINDy method, the right-hand side of the original dynamical system $f(q(t))$, which is a nonlinear function of the state variable q, is approximated by a linear relationship as $f(q(t)) \approx \boldsymbol{\theta}(q(t))\boldsymbol{\xi}$, where the matrix $\boldsymbol{\theta}(q)$ is a library of some candidate nonlinear functions of the coordinates of the systems q, such as $\boldsymbol{\theta}(q) = [Iq^1q^2\ldots q^d\ldots \sin q\ldots]$ to incorporate the nonlinearity. The columns of the coefficients matrix $\boldsymbol{\xi}$ can be determined using a convex sparse regression: $\xi_k = \mathrm{argmin}_{\xi_k'}\left\|\dot{\boldsymbol{Q}}_k - \boldsymbol{\theta}(\boldsymbol{Q})\xi_k'\right\|_2 + \lambda\|\xi_k\|_1$ where $\dot{\boldsymbol{Q}}_k$ is the k^{th} column of $\dot{\boldsymbol{Q}}$, $\boldsymbol{Q}$ is the snapshots matrix of the training data, $\|\ldots\|_1$ and $\|\ldots\|_2$ are the l_2-norm and l_1-norm of the matrix, respectively, and λ is a sparsity-promoting penalty parameter. Then, the original dynamical system can be approximated by using the library as $\dot{q} = \boldsymbol{\theta}(q)\boldsymbol{\xi}$. For the applications of fluid dynamics, the SINDy algorithm is usually combined with a dimensional reduction as prior. For example, Kaptanoglu et al. [59], Loiseau et al. [60], and Callaham et al. [61] performed the POD analysis and then used the SINDy to predict the temporal evolution of the POD coefficients $\boldsymbol{a}(t)$ for magnetohydrodynamics, cavity flows, mixing layer, and cylinders wake flows. Fukami et al. [62] used CNN based autoencoder to map the wake flow data behind a cylinder onto a 2D latent space and adopted the SINDy to predict the dynamics of the latent space and reconstruct the predicted flows at future time steps.

Furthermore, recurrent NNs (RNN), as a popular tool for processing sequential data such as video images and natural language, are specifically appropriate for predicting the temporal evolution of FSI systems. However, RNNs have the problems of vanishing gradient and cannot learn long-term dependencies in the data sequences. Therefore, Hochreiter et al. [63] developed long short-term memory (LSTM) networks, where a gating mechanism controls the dynamics of the recurrent connections, to mitigate the issue of vanishing gradient and predict the long temporal dependencies. Combining with the POD analysis, LSTM can be also used to predict the temporal evolution of the POD coefficients $\boldsymbol{a}(t)$ as shown in Nazvanova et al. [64] for a VIV cylinder at high Re. A predictive model in combination of CNN and LSTM can be developed to predict the temporal evolution of the unsteady flow over a side-by-side cylinder by Bukka et al. [65] and Gupta et al. [66, 67]. A framework of this prediction method is shown in Fig. 7. The snapshots of flow fields $\boldsymbol{X} = [\boldsymbol{u}(x,t_1), \boldsymbol{u}(x,t_2), \ldots, \boldsymbol{u}(x,t_N)]$ are used as the training data and are compressed into low-dimensional latent space states of $\boldsymbol{Z} = [z(t_1), z(t_2), \ldots, z(t_N)]$ using the encoder. Then, LSTM is built to model the temporal evolution of the low-dimensional states advancing from $[z(t_1), z(t_2), \ldots, z(t_N)]$ to $[z(t_2), z(t_3), \ldots, z(t_{N+1})]$. Finally, the full flow states at the future time instants can be reconstructed from the low-dimensional latent states. It should be mentioned that this architecture combining CNN and LSTM could be generalized to any FSI system.

Transformer NNs, an advanced sequence-to-sequence architecture, significantly improve the efficiency of processing natural language [68, 69] and can be also adopted for temporal-dynamics prediction of the latent space. The transformer NN architecture consists of an encoder and a decoder between the input and output sequences and uses the attention mechanism to extract global dependencies between the two sequences. Wang et al. [70] and Solera-Rico et al. [71] employed a CNN-β-VAE model to encode the domain name system (DNS) data of turbulent flow around a wall-mounted square cylinder and two collinear flat plates (Fig. 8). Then, the transformer to predict the temporal-dynamics. It showed that the chaotic evolutions of the latent space states were predicted with a more satisfactory accuracy compared with the LSTM model.

4.3 Control of FSI

Upon gaining a physical understanding and prediction of the FSI

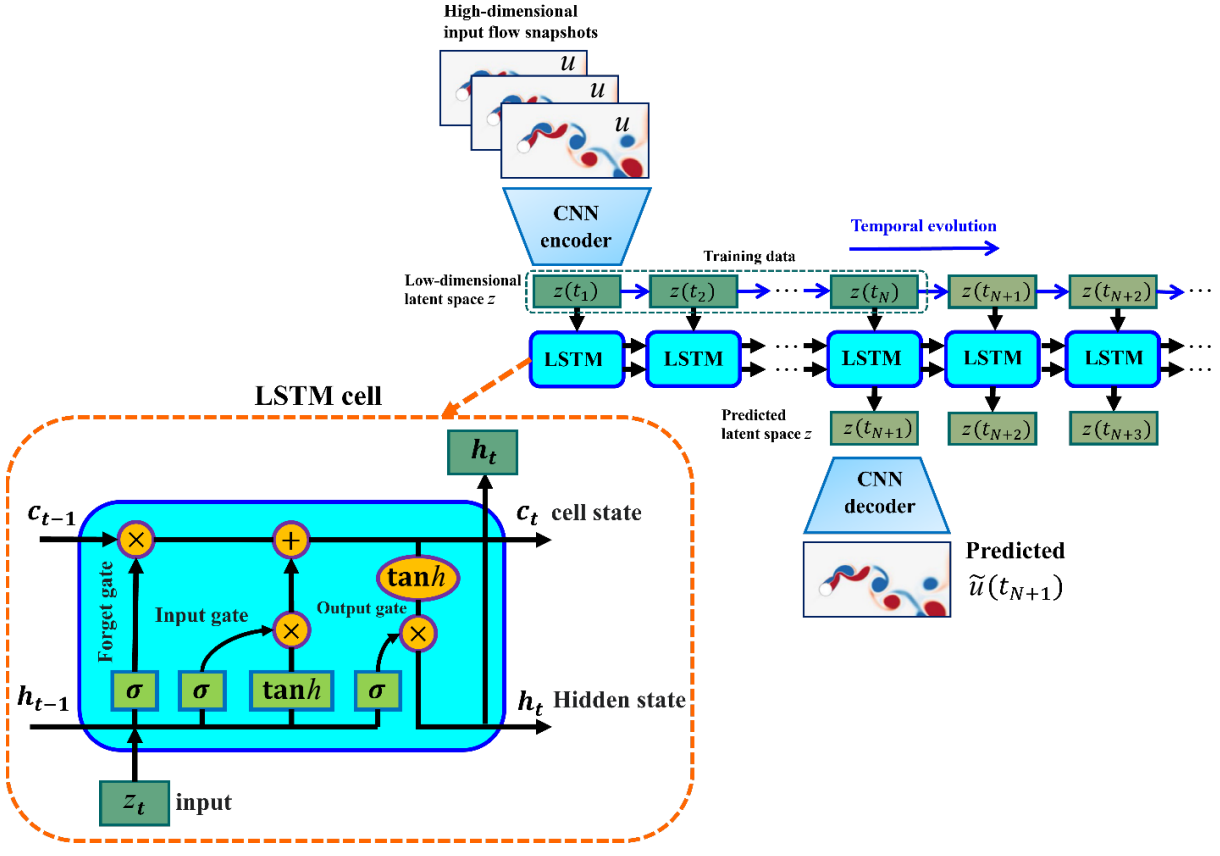

Figure 7 A schematic view of the CNN combined LSTM prediction method of FSI systems and the cell structure of the LSTM.

dynamics, the subsequent crucial problem is how to develop efficient control strategies for FSI. Especially for engineering applications, there exist multiple control objectives. For instance, in ocean engineering, slender structures like marine risers are prone to fatigue-related damage due to large-amplitude flow-induced-vibrations, which requires control methods to suppress the vibrations. On the other hand, for renewable energy such as wave-energy converters [72] and hydrokinetic energy harnessing systems such as VIV aquatic clean energy (VIVACE) converters [73], it is necessary to enhance the structural response so as to increase the power transfer and the utilization efficient.

Traditionally, FSI control is achieved via passive control dependent on modifications of structural geometries, which lacks adaptability and scalability under various environmental conditions. Therefore, active flow control emerges as a hotspot in FSI control. The active control uses external control inputs such as structural self-rotating, surface morphology, or opposite control forces. As a typical active control, close-loop or feedback control can provide a rigorous mathematical plant to achieve an efficient way by entering control signals through actuators while conducting real-time systems estimation using sensors. The FSI control always encounters the problems of nonlinearity and high-dimensionality due to the nature of FSI systems. Thus, a linearization of the governing equations is always performed through either linearization around the system trajectory or the mean systems state. Some examples of this method can be found in Semeraro et al. [74] and Semeraro et al. [75]. Nevertheless, in real industries, it is difficult to mathematically derive simple linear-model-based control schemes neglecting nonlinearity, especially when there are complicated couplings between fluids and structures. Furthermore, multiscale features such as turbulence pose difficulties to control problems. These important physical phenomena cannot be simply incorporated into the first-principle governing equations of the control systems. Fortunately, ML and deep learning [76] provide new opportunities for FSI control.

Nowadays, reinforcement learning (RL), which has been widely applied in automated driving and game playing, becomes popular in FSI control. In general, the framework of RL control regards the numerical simulations or experiments of any FSI system as an "environment" and trains the control "agent" by interacting with this environment through three channels: the observation signals o_t, the action a_t, and the reward r_t. The observation signals are usually pointwise measurements of flow quantities such as flow velocities and pressures in the flow fields. The action refers to the active control signals such as suction or blowing of the synthetic jet flows placed on the structure surfaces. The reward is usually related to the control objective. For example, for the common drag reduction control problems of bluff bodies as shown in Rabault et al. [77], Tang et al. [78], Varela et al. [79], and Ren et al. [80], the reward can be the time-averaged drag coefficient of the structures. A schematic of the RL framework is shown in Fig. 9. For enhancing heat transfer in energy and power engineering, the reward can be the time-averaged integral of the local temperature gradient along the structure surfaces as reported in Ren et al. [80]. The agent is usually a NN trained to seek a control strategy to determine at based on o_t at the current time step, aiming to maximize the reward r_t.

RL can be generally divided into model-free and model-based methods. The model-free method is the most commonly used algorithm for FSI control problems, which can be further classified

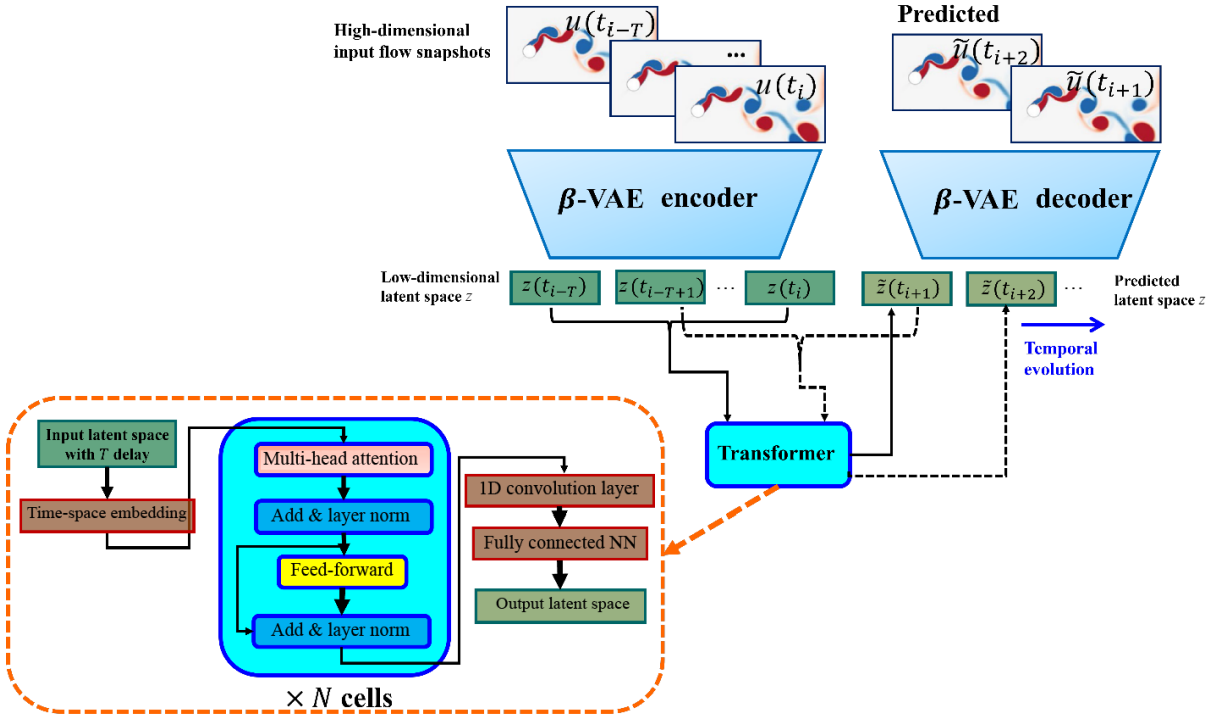

Figure 8 A schematic view of the CNN-β-VAE model combined with the transformer prediction method of FSI systems.

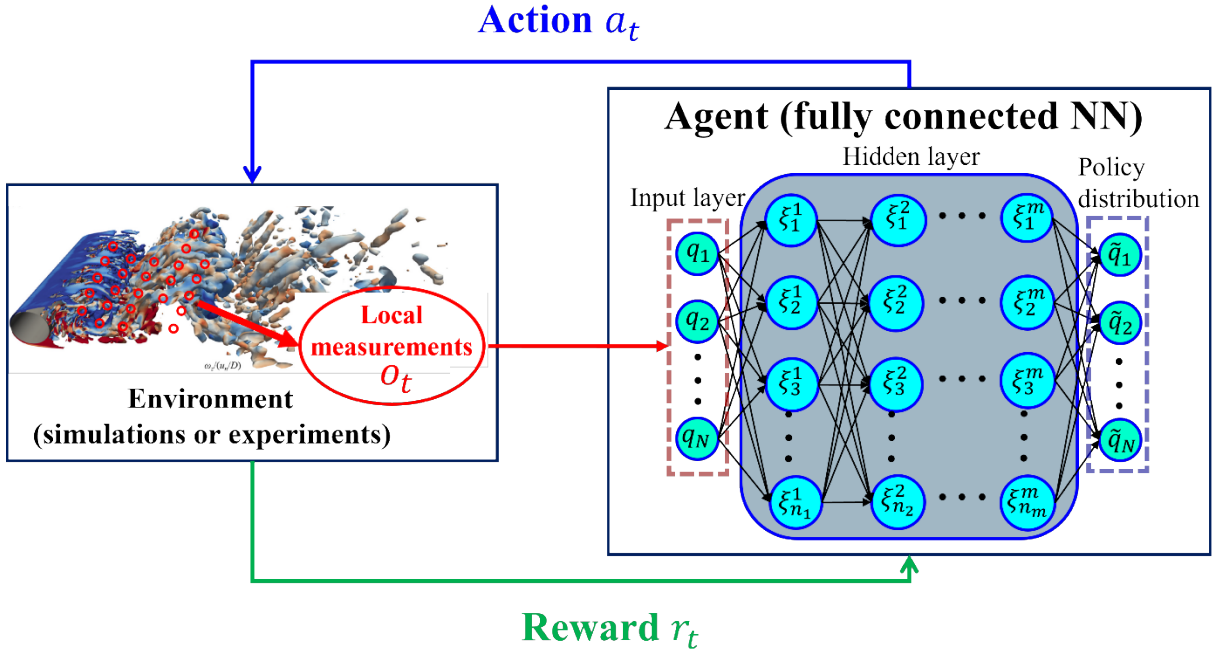

Figure 9 Schematic of the RL loop framework. Agent, NN. The environment usually refers to numerical simulations or experiments. The synthetic jet flow rates and plasma actuators are commonly used as action. Reduction in the time-averaged hydrodynamic forces is acting as the reward. The pointwise measurements of the flow velocity are usually the observations.

into value-based (i.e., the classic Q-learning) and policy-based methods. As summarized by Garnier et al. [81], compared with the valued-based methods, the policy-based methods, also known as policy gradient methods, have advantages of dealing with high dimensional action spaces and have better stability and convergence properties.

In Rabault et al. [77], a deep RL (DRL) technique was developed combining with NNs. The aim of the developed DRL is to obtain the optimal policy $\pi(a_t|o_t)$, which is described as the probability distribution of action a_t given the observation o_t for maximizing the cumulative reward $R(t) = \sum_{i>t}\gamma^{i-t}r_t$, where γ is the discount factor. The proximal policy optimization (PPO), one of the policy

gradient methods, was employed to learn the parameter set denoted as Θ of NN such as to maximize the expected reward given as

$$R_{\max} = \max \mathbb{E}\left[\sum_{t=0}^{H} R(s_t)|\pi_\Theta\right] \quad (3)$$

where π_Θ is the policy represented by NN with the parameter set Θ, and s_t is the system state (i.e., the flow state) represented by the observation o_t at the time t. The maximization is achieved by using the gradient descent algorithm on the parameter set Θ.

Rabault et al. [77] applied the DRL to learn an active control strategy and obtain the mass flow rates of the synthetic jet on a cylinder surface subjected to a laminar flow at $Re = 100$. The vortex shedding was suppressed, and the drag was reduced by 8%. Also, the lift and drag fluctuations were also significantly reduced at a series of Reynolds number ranging between 60 and 400 as reported in Tang et al. [78]. Apart from control by using the surface jet flows, the DRL-based drag reduction was also achieved using rotational oscillations of a cylinder by Han et al. [82]. Two small counter-rotating cylinders located at the back of the main cylinder were used in studies by Xu et al. [83] and Fan et al. [84] to stabilize the vortex shedding, and the rotating speed was determined by the artificial neural network (ANN) combined DRL. The linear stability of the wake flow behind a cylinder confined between two plates was investigated, and the vortex shedding was stabilized using RL control strategy by Li et al. [85]. Yousif et al. [86] developed a DRL control strategy combined with PPO to control the flow around a square cylinder using a plasma actuator as the control signal. The lift and drag coefficients were reduced and the aerodynamic stability of the cylinder was enhanced.

4.4 Physics-informed NNs (PINNs) of FSI

Modern ML and deep learning techniques are primarily data-driven, relying on extensive datasets to extract physically meaningful patterns. However, in practical experiments and real-world industrial applications, observational and measurement data are often limited and sparse, therefore constraining the predictive capacity of NNs trained upon such data. Furthermore, despite the broad applications of these techniques, the core models such as MLPs and CNNs typically lack interpretability and explainability. Given the fact that almost all investigated dynamic systems in science and engineering are governed by first-principle physical laws, these challenges motivate the development of PINNs by Raissi et al. [87] for solving PDEs using NN.

In the framework of PINN, different from traditional numerical methods for solving PDEs such as the finite difference method and the finite volume method, the automatic differentiation (AD) is employed in PINN to represent all the differential operators in PDEs instead of discretization methods. Therefore, there is no requirement for computational meshes. The temporal and the spatial coordinates (x,t) are regarded as the inputs, and the solution state vector $\boldsymbol{u}(x,t)$ of the underlying governing PDE represented as $u_t + N(\boldsymbol{u}) = 0$ ($N(\boldsymbol{u})$ includes all linear and nonlinear differential operators regarding $\boldsymbol{u}(x,t)$) is the output. A typical PINN usually consists of a DNN built by an MLP mapping the inputs of the spatial and temporal coordinates to the solution $\boldsymbol{u}(x,t)$ of the PDE. The weights and biases of the MLP are obtained through the training process for minimizing the loss function, which consists of both supervised loss and residual of the governing equations. The supervised loss refers to the differences between the predicted solutions and the available training data in sample points at the domain boundaries and inside the domains. The physical constraints are primarily incorporated as the residual of the governing PDEs represented as $L_{\text{PDE}} = \sum_{i=1}^{N_e} |u_{i,t} + N(u_i)|^2$ at N_e points (known as collocation points) for which the residual of the

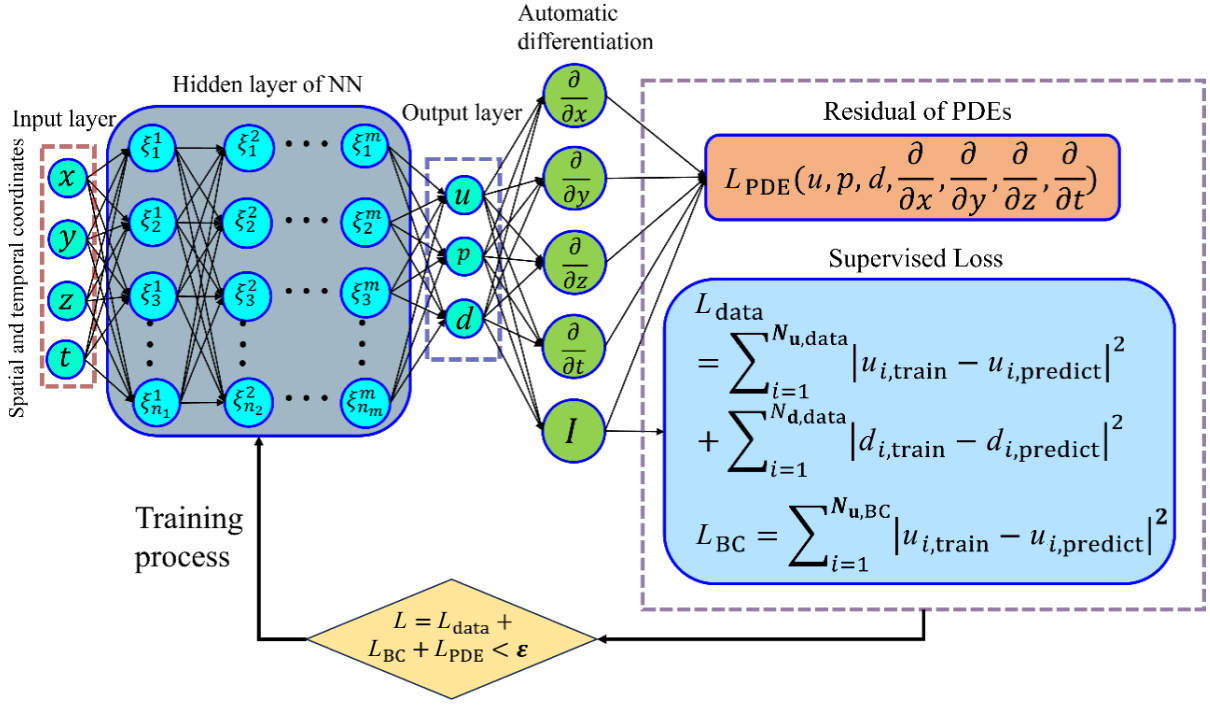

Figure 10 Schematic of a PINN. An FCN uses time and space coordinates (x,y,z,t) as inputs to solve the multi-physics solutions including the flow data (u,p) and also structural responses (d). The spatial and temporal derivatives of the solution quantities with respect to the inputs are calculated using AD of the FCN and then used to formulate the residuals of the governing PDE and supervised loss inside the computational domain and at the boundaries in the loss function. The parameters of the FCN are trained by minimizing the loss function.

https://doi.org/10.26599/OCEAN.2025.9470002

governing PDEs is calculated. A framework of a typical PINN is presented in Fig. 10. It should be mentioned that AD combined with the chain rule is used to compute the gradients of the solution variables with respect to the spatial and temporal coordinates in the governing PDEs in a forward manner and update the parameters of NN in the backpropagation process.

Since it was introduced by Raissi et al. [87], PINN has been successfully applied for both forward and inverse problems governed different types of PDEs from one-dimensional (1D) Burges' equations to 3D NS equations for fluids. The forward problems aim at predicting the PDE solutions at sample points while the inverse problems identify and infer critical parameters or boundary conditions of the PDEs based on the training data. PINNs showed good performance in solving the Reynolds-averaged NS (RANS) equations for incompressible turbulent boundary layer flows and turbulent flows over a NACA4412 airfoil and periodic hills. The Reynolds stress is well predicted by using PINN compared with simulation results. Classic bluff body flow problems such as 2D laminar flows around a circular cylinder were also considered in Raissi et al. [87], Rao et al. [88], Jin et al. [89], and Yan et al. [90]. 3D flows were also reconstructed using limited data combined with PINN by Cai et al. [91] and Xu et al. [92]. In addition, PINN has become a popular tool for high-resolution reconstruction of flow data from low-resolution, incomplete and noisy measurements as shown in Eivazi et al. [93]. For FSI problems involving moving structure surfaces, the motions of the structures should also be incorporated in the governing NS equations. Typical examples can be found in Raissi et al. [94], Cheng et al. [95], Bai et al. [96], and Tang et al. [97]. In these applications for a VIV cylinder, the NS equations in the coordinate system attached to the vibrating cylinder were considered by adding the acceleration of the cylinder in the equations. The lift and drag forces of the cylinder can be predicted using the sparse velocity measurements combined with the PINN.

5 Challenges

Despite the broad applications of ML in FSI and other flow problems, its development has predominantly been within the realm of model studies, which means that the performances of ML are typically evaluated using flows over simple geometries such as cylindrical and spherical structures at low Reynolds numbers and other canonical flow problems, such as channel flow, pipe flow, and boundary layer flow. There is a noticeable shortage in the availability of ML capable of dealing with complicated real-world FSI problems in ocean engineering and industrial settings including wind turbines, subsea pipelines, and vibrating and flapping hydrofoils. The primary challenges and potential solutions for applying ML to these FSI problems are outlined in this section.

5.1 Interaction between structures and fluid flows

For typical FSI problems, strong nonlinear coupling exists between the structural responses such as motions and deformations of structures and the coherent flow structures. A critical phenomenon within these interactions is the synchronization which occurs when the natural frequency of the structure matches the characteristic frequency of the coherent flow structures, such as vortex shedding frequency. This synchronization, often referred to as a lock-in regime, can induce significantly large structural displacement amplitude and a complex interchange of energy between the structure and the surrounding flow, which is highly dependent on timescales and phase alignment between the structure displacements and flow-induced forces [40]. A deforming computational mesh in a body-fitted frame is typically used for feature detection since decoupling the moving body-fitted frame from the flow is necessary. Existing ML for FSI often deals with structures with prescribed motions and some examples can be seen in Menon et al. [98, 99]. In these cases, the deformation of the moving mesh is presupposed. When it comes to structures that move freely within a fluid, the focus has primarily been on thin structures, as discussed in Stankiewicz et al. [100]. Furthermore, to build the Galerkin-projection ROM, the structural motions and deformations based on ALE were considered by Stankiewicz et al. [100]. However, applying ALE to FSI systems with large structural displacements proves challenging, highlighting a requirement of an efficient ML methodology that can accurately capture and predict the nonlinear FSI interaction with large amplitude motions and high unsteadiness of associated flow-induced forces.

5.2 Strong nonlinearity of the dynamical systems

One of the most important features of the FSI systems lies in their strong nonlinearity, making their analysis particularly challenging. Current methods to analyse nonlinear systems usually approximate the nonlinear system with linear system in a small neighbourhood of a fixed point of a periodic orbit, such as classic linear stability theory [101], allowing for the applications of well-established linear analysis techniques and control schemes. However, this linear approximation can only discern local characteristics of the original systems and fails to capture global nonlinear characteristics. The periodic or quasi-periodic behaviour of nonlinear systems can be characterized using the DMD modal analysis based on the Koopman operator [33]. The key assumption of DMD modal analysis is that while the dynamical system might be nonlinear, the evolution of the observables under the Koopman operator is linear. Despite of the frequency information provided by DMD, this approach encounters limitations when faced with intricate nonlinear phenomena often seen in turbulence: transients, intermittency, and broadband spatial and temporal scale distributions. These features cannot be fully captured using only the linear expansions of Koopman modes. While CNN and DNN are capable of incorporating nonlinearity within the latent space, their utilization hinges on the nonlinear properties of activation functions at each node in the hidden layers. The absence of correlations with the nonlinear aspects of FSI remains a crucial aspect, and these correlations are crucial for developing ROMs which not only simplify the representation of complex FSI systems but also illuminate the fundamental mechanisms.

5.3 Unresolved flow physics

In ocean engineering, flows are characterized by their Reynolds number, a critical parameter that determines different flow regimes. As elucidated in classical turbulence theory, an increase in the Reynolds number leads to a proliferation of spatial and temporal scales within the flow and subsequently generates complex motion patterns of structures immersed within these flows [40]. ML techniques, particularly feature detection algorithms, provide a way to decrease the dimensionality and reduce the complexity of the problems. Nevertheless, one of the consequences is that only dynamics with large spatiotemporal scales is retained, and small-scale dynamics becomes unresolved. However, these small-scale

unresolved motions may be crucial to the kinetic energy dissipation process of the systems. For the evolvement of the dynamical systems, this energy dissipation is important for maintaining the realistic energy cascade in the flow and system stability, which should be carefully considered in the ML techniques. This concept is in resemble to the turbulence closure models when carrying out RANS or large eddy simulations (LES) and the POD projection-based models by Podvin et al. [23] and Podvin [24].

5.4 Unidealized and realistic structural shapes and configurations

The limited success of ML applications in addressing real-world FSI problems in industries can be largely attributed to the unidealized structural shapes instead of simplified bodies in academic research and their complicated configurations when multiple structures are presented. For example, in offshore engineering, there are various forms of wind turbine designs, each presenting unique FSI patterns due to distinct wake flow interactions. In subsea engineering, the proximity of risers and piggyback pipelines introduces intricate vortex shedding patterns, increasing difficulty in applying ML to such systems. Attempts to address these problems can be found in Miyanawala et al. [102] and Yao et al. [103]. However, they are still restricted to bodies with idealized shapes.

5.5 Hydrodynamic or aerodynamic loads on structures

Accurately predicting unsteady loads with high amplitudes on structures in engineering applications is crucial for ensuring structural integrity, stability, and prolonging fatigue life. Typically, these loads are determined in FSI simulations by integrating pressure and shear stress data collected on the surfaces of structures. However, acquiring flow quantities directly from these surfaces is challenging in real-world scenarios, and installing load measurement devices might undesirably influence the surrounding flow field. An alternative strategy involves estimating the loads directly from the surrounding flow information, leveraging the momentum transfer between the moving structures and the fluid. Relevant estimation methods such as FPM can be found in Menon et al. [39], Tong et al. [104], Yin et al. [41], and Nazvanova et al. [64]. However, in applications of ML, it is still unknown how to relate the flow features encoded in the latent space to the loads on the structures and how individual flow feature and their mutual interactions contribute to the loads. Current methods for estimating loads depend heavily on having complete and spatially continuous data on surrounding flow fields. However, obtaining such extensive flow field measurements in practical scenarios is often infeasible due to the prohibited costs associated with experimental setups and data storage. This raises the challenge of how to effectively use the limited and sparse available data to estimate the complete flow information, and subsequently, the loads, particularly in FSI systems.

6 Summary and recommendations

This paper presents a comprehensive review of the latest developments of ML techniques for FSI. Traditional methodologies of FSI research are briefly overviewed and then ML is introduced. Specific applications of ML on FSI problems are generally classified into three primary directions and relevant techniques and algorithms are discussed. The subsequent section focuses on the existing challenges in applying ML in FSI. Some recommendations for current and future development are outlined as follows.

6.1 Overcoming the challenges of moving structures

In CFD simulations, accurately capturing moving structures and their interaction with fluid flows presents challenges. This complexity arises because these simulations necessitate additional computations for the structural responses and often pose difficulties with stability issues. When it comes to experimental investigations, moving structures introduce uncertainties in the measurement data. The majority of ML applications in FSI have focused on flows over stationary structures. The traditional view of flow problems is mostly based on Eulerian perspective, where a fixed reference frame and fixed computational mesh are employed. However, for FSI systems, there is a compelling case for adopting the Lagrangian description, where the movement of specific material points is followed in a moving reference frame. It is crucial to explore both descriptions and their respective merits within the framework of ML for specific FSI problems.

6.2 Incorporate physical constraints

Despite the proliferation of deep learning, RL, and artificial intelligence, their primary applications have been in the fields such as business, finance, climate and neuroscience, characterized by "soft constraints". These fields often deal with probabilistic and flexible frameworks. In contrast, disciplines such as physics, chemistry, civil, offshore, and mechanical engineering are governed by "hard constraints" rooted in physical laws. This means that the developed ML techniques should inherently respect the fundamental physical laws governing FSI systems. Although various PINN architectures incorporated the governing PDEs into the training process, more physical laws encompassing momentum and energy conservations, divergence-free criteria for incompressible fluid velocity fields, no-slip boundary conditions on structural surfaces, consistency between pressure and velocity fields, and strain compatibility of elastic structures should also be considered. Furthermore, there are still limitations when applying PINN in FSI investigations. The predominant focus of PINN applications on FSI problems is on steady-state flow predictions such as Eivazi et al. [93], Hanrahan et al. [105], and Patel et al. [106]. The prediction ability of PINNs for flows with unsteady characteristics, even as elementary as vortex shedding at low Reynolds number remains questionable as reported by Chuang et al. [107]. The unsteady flow decays to a steady flow if there are no available training data, which indicates high numerical dispersion and diffusion of PINN. Thus, how to effectively address and reasonably incorporate the "hard constraints" in FSI systems is an important research direction.

6.3 Bridge the gap between mathematical tools and real industrial applications.

The development of ML is heavily reliant on mathematical methodologies. A central consideration in both science and engineering is how to translate these mathematical theories to real-world applications, and conversely, abstracting complex industrial situations into fundamental elements for mathematical modelling. This dual process highlights the needs to bridge the gap between the mathematical tools for simplified and idealized FSI problems and their practical implementation in ocean and offshore engineering. To effectively address this gap, it is important to develop an interdisciplinary approach that merges insights and methodologies from diverse fields such as applied mathematics,

https://doi.org/10.26599/OCEAN.2025.9470002

ML, big data analytics, control theory, and structural mechanics. By integrating knowledge from these areas, the development of ML models can be significantly enhanced, not only with increasing their accuracy in predicting and solving complex FSI problems but also increasing transfer ability.

Acknowledgements

None.

Author contribution statement

Muk Chen Ong: Conceptualization; Writing – original draft; Data curation; Formal Analysis; Methodology; Writing – review & editing. Guang Yin: Conceptualization; Writing – original draft; Data curation; Formal Analysis; Methodology; Writing – review & editing. Both authors have approved the final manuscript.

Data availability

Not applicable.

Declaration of competing interest

All the contributing authors report no conflict of interests in this work.

Funding

None.

Use of AI statement

None.

References

[1] Liu, Y. C., Xiao, Q., Incecik, A., Peyrard, C., Wan, D. C. (2017). Establishing a fully coupled CFD analysis tool for floating offshore wind turbines. *Renew. Energy* 112, 280–301.

[2] Janocha, M. J., Ong, M. C., Yin, G. (2022). Large eddy simulations and modal decomposition analysis of flow past a cylinder subject to flow-induced vibration. *Phys. Fluids* 34, 045119.

[3] Posa, A. (2023). End effects in the wake of a hydrofoil working downstream of a propeller. *Phys. Fluids* 35, 045122.

[4] Wang, Z. K., Yin, G., Ong, M. C., Chen, Y. (2023). Improved delayed detached eddy simulations of flow past an autonomous underwater helicopter. *Phys. Fluids* 35, 075144.

[5] Cheng, H., Ong, M. C., Li, L., Chen, H. (2022). Development of a coupling algorithm for fluid-structure interaction analysis of submerged aquaculture nets. *Ocean Eng* 243, 110208.

[6] Kinsey, T., Dumas, G. (2008). Parametric study of an oscillating airfoil in a power-extraction regime. *AIAA J* 46, 1318–1330.

[7] Xiao, Q., Liao, W., Yang, S. C., Peng, Y. (2012). How motion trajectory affects energy extraction performance of a biomimic energy generator with an oscillating foil?. *Renew. Energy* 37, 61–75.

[8] Xiao, Q., Zhu, Q. (2014). A review on flow energy harvesters based on flapping foils. *J. Fluids Struct* 46, 174–191.

[9] Pope, S. B. (2001). Turbulent flows. *Meas. Sci. Technol* 12, 2020.

[10] Gsell, S., Bourguet, R., Braza, M. (2016). Two-degree-of-freedom vortex-induced vibrations of a circular cylinder at *Re*= 3900. *J. Fluids Struct* 67, 156–172.

[11] Mendez, M. A., Ianiro, A., Noack, B. R., Brunton, S. L. (2023). Data-Driven Fluid Mechanics: Combining First Principles and Machine Learning. Cambridge: Cambridge University Press.

[12] Schölkopf, B., Smola, A. J. (2002). Learning with Kernels: Support Vector Machines, Regularization, Optimization, and Beyond. Cambridge: MIT Press.

[13] Breiman, L. (2001). Random forests. *Mach. Learn* 45, 5–32.

[14] Cover, T., Hart, P. (1967). Nearest neighbor pattern classification. *IEEE Trans. Inform. Theory* 13, 21–27.

[15] Xu, Q., Li, W. S., Liu, W. Z., Zhang, X. M., Yang, C. Y., Guo, L. J. (2020). Intelligent recognition of severe slugging in a long-distance pipeline-riser system. *Exp. Therm. Fluid Sci* 113, 110022.

[16] Li, W. H., Song, W. R., Yin, G., Ong, M. C., Han, F. H. (2022). Flow regime identification in the subsea jumper based on electrical capacitance tomography and convolution neural network. *Ocean Eng* 266, 113152.

[17] Duraisamy, K., Iaccarino, G., Xiao, H. (2019). Turbulence modeling in the age of data. *Annu. Rev. Fluid Mech* 51, 357–377.

[18] Tracey, B., Duraisamy, K., Alonso, J. (2013). Application of supervised learning to quantify uncertainties in turbulence and combustion modeling. In Proceedings of the 51st AIAA Aerospace Sciences Meeting Including the New Horizons Forum and Aerospace Exposition. Grapevine, p 259.

[19] Kužnar, D., Možina, M., Giordanino, M., Bratko, I. (2012). Improving vehicle aeroacoustics using machine learning. *Eng. Appl. Artif. Intell* 25, 1053–1061.

[20] Raul, V., Leifsson, L. (2021). Surrogate-based aerodynamic shape optimization for delaying airfoil dynamic stall using Kriging regression and infill criteria. *Aerosp. Sci. Technol* 111, 106555.

[21] Lumley, J. L. (1967). The structure of inhomogeneous turbulent flows. *Atmos. Turbul. Radio Wave Propag* 1967, 166–178.

[22] Ilak, M., Rowley, C. W. (2008). Modeling of transitional channel flow using balanced proper orthogonal decomposition. *Phys. Fluids* 20, 034103.

[23] Podvin, B., Lumley, J. (1998). A low-dimensional approach for the minimal flow unit. *J. Fluid Mech* 362, 121–155.

[24] Podvin, B. (2009). A proper-orthogonal-decomposition–based model for the wall layer of a turbulent channel flow. *Phys. Fluids* 21, 015111.

[25] Rowley, C. W., Colonius, T., Murray, R. M. (2004). Model reduction for compressible flows using POD and Galerkin projection. *Phys. D: Nonlinear Phenom* 189, 115–129.

[26] Liberge, E., Hamdouni, A. (2010). Reduced order modelling method via proper orthogonal decomposition (POD) for flow around an oscillating cylinder. *J. Fluids Struct* 26, 292–311.

[27] Riches, G., Martinuzzi, R., Morton, C. (2018). Proper orthogonal decomposition analysis of a circular cylinder undergoing vortex-induced vibrations. *Phys. Fluids* 30, 105103.

[28] Towne, A., Schmidt, O. T., Colonius, T. (2018). Spectral proper orthogonal decomposition and its relationship to dynamic mode decomposition and resolvent analysis. *J. Fluid Mech* 847, 821–867.

[29] Schmidt, O. T., Towne, A., Rigas, G., Colonius, T., Brès, G. A. (2018). Spectral analysis of jet turbulence. *J. Fluid Mech* 855, 953–982.

[30] Schmidt, O. T., Colonius, T. (2020). Guide to spectral proper orthogonal decomposition. *AIAA J* 58, 1023–1033.

[31] Nidhan, S., Schmidt, O. T., Sarkar, S. (2022). Analysis of coherence in turbulent stratified wakes using spectral proper orthogonal decomposition. *J. Fluid Mech* 934, A12.

[32] Mendez, M. A., Balabane, M., Buchlin, J. M. (2019). Multi-scale proper orthogonal decomposition of complex fluid flows. *J. Fluid Mech* 870, 988–1036.

[33] Schmid, P. J. (2010). Dynamic mode decomposition of numerical and experimental data. *J. Fluid Mech* 656, 5–28.

[34] Kou, J. Q., Zhang, W. W. (2017). An improved criterion to select dominant modes from dynamic mode decomposition. *Eur. J. Mech. - B/Fluids* 62, 109–129.

[35] Kou, J. Q., Le Clainche, S., Zhang, W. W. (2018). A reduced-order model for compressible flows with buffeting condition using higher order dynamic mode decomposition with a mode selection criterion. *Phys. Fluids* 30, 016103.
[36] Jovanović, M. R., Schmid, P. J., Nichols, J. W. (2014). Sparsity-promoting dynamic mode decomposition. *Phys. Fluids* 26, 024103.
[37] Le Clainche, S., Vega, J. M. (2017). Higher order dynamic mode decomposition. *SIAM J. Appl. Dyn. Syst* 16, 882–925.
[38] Chang, C. C. (1992). Potential flow and forces for incompressible viscous flow. *Proc. Roy. Soc. A: Math. Phys. Eng. Sci* 437, 517–525.
[39] Menon, K., Mittal, R. (2021). On the initiation and sustenance of flow-induced vibration of cylinders: Insights from force partitioning. *J. Fluid Mech* 907, A37.
[40] Menon, K., Mittal, R. (2021). Significance of the strain-dominated region around a vortex on induced aerodynamic loads. *J. Fluid Mech* 918, R3.
[41] Yin, G., Janocha, M. J., Ong, M. C. (2022). Estimation of hydrodynamic forces on cylinders undergoing flow-induced vibrations based on modal analysis. *J. Offshore Mech. Arct. Eng* 144, 060904.
[42] Lecun, Y., Bottou, L., Bengio, Y., Haffner, P. (1998). Gradient-based learning applied to document recognition. *Proc. IEEE* 86, 2278–2324.
[43] Murata, T., Fukami, K., Fukagata, K. (2020). Nonlinear mode decomposition with convolutional neural networks for fluid dynamics. *J. Fluid Mech* 882, A13.
[44] Fukami, K., Nakamura, T., Fukagata, K. (2020). Convolutional neural network based hierarchical autoencoder for nonlinear mode decomposition of fluid field data. *Phys. Fluids* 32, 095110.
[45] Guastoni, L., Güemes, A., Ianiro, A., Discetti, S., Schlatter, P., Azizpour, H., Vinuesa, R. (2021). Convolutional-network models to predict wall-bounded turbulence from wall quantities. *J. Fluid Mech* 928, A27.
[46] Yousif, M. Z., Yu, L. Q., Hoyas, S., Vinuesa, R., Lim, H. (2023). A deep-learning approach for reconstructing 3D turbulent flows from 2D observation data. *Sci. Rep* 13, 2529.
[47] Güemes, A., Discetti, S., Ianiro, A., Sirmacek, B., Azizpour, H., Vinuesa, R. (2021). From coarse wall measurements to turbulent velocity fields through deep learning. *Phys. Fluids* 33, 075121.
[48] Kingma, D. P., Welling, M. (2013). Auto-encoding variational bayes. arXiv preprint arXiv:1312.6114.
[49] Higgins, I., Matthey, L., Pal, A., Burgess, C., Glorot, X., Botvinick, M., Mohamed, S., Lerchner, A. (2017). β-VAE: Learning basic visual concepts with a constrained variational framework. In Proceedings of the 5th International Conference on Learning Representations. Toulon.
[50] Eivazi, H., Tahani, M., Schlatter, P., Vinuesa, R. (2022). Physics-informed neural networks for solving Reynolds-averaged Navier–Stokes equations. *Phys. Fluids* 34, 075117.
[51] Rowley, C. W. (2005). Model reduction for fluids, using balanced proper orthogonal decomposition. *Int. J. Bifurcation Chaos* 15, 997–1013.
[52] Östh, J., Noack, B. R., Krajnović, S., Barros, D., Borée, J. (2014). On the need for a nonlinear subscale turbulence term in POD models as exemplified for a high-Reynolds-number flow over an Ahmed body. *J. Fluid Mech* 747, 518–544.
[53] Podvin, B., Pellerin, S., Fraigneau, Y., Evrard, A., Cadot, O. (2020). Proper orthogonal decomposition analysis and modelling of the wake deviation behind a squareback Ahmed body. *Phys. Rev. Fluids* 5, 064612.
[54] Podvin, B., Pellerin, S., Fraigneau, Y., Bonnavion, G., Cadot, O. (2021). Low-order modelling of the wake dynamics of an Ahmed body. *J. Fluid Mech* 927, R6.
[55] Podvin, B., Pellerin, S., Fraigneau, Y., Bonnavion, G., Cadot, O. (2022). Relationship between the base pressure and the velocity in the near-wake of an Ahmed body. *Phys. Rev. Fluids* 7, 054602.
[56] Dadfar, R., Hanifi, A., Henningson, D. S. (2015). Feedback control for laminarization of flow over wings. *Flow, Turbul. Combust* 94, 43–62.
[57] Bagheri, S. (2013). Koopman-mode decomposition of the cylinder wake. *J. Fluid Mech* 726, 596–623.
[58] Sharma, A. S., Mezić, I., McKeon, B. J. (2016). Correspondence between Koopman mode decomposition, resolvent mode decomposition, and invariant solutions of the Navier-Stokes equations. *Phys Rev Fluids* 1, 032402.
[59] Kaptanoglu, A. A., Morgan, K. D., Hansen, C. J., Brunton, S. L. (2021). Physics-constrained, low-dimensional models for magnetohydrodynamics: First-principles and data-driven approaches. *Phys. Rev. E* 104, 015206.
[60] Loiseau, J. C., Brunton, S. L. (2018). Constrained sparse Galerkin regression. *J. Fluid Mech* 838, 42–67.
[61] Callaham, J. L., Brunton, S. L., Loiseau, J. C. (2022). On the role of nonlinear correlations in reduced-order modelling. *J. Fluid Mech* 938, A1.
[62] Fukami, K., Murata, T., Zhang, K., Fukagata, K. (2021). Sparse identification of nonlinear dynamics with low-dimensionalized flow representations. *J. Fluid Mech* 926, A10.
[63] Hochreiter, S., Schmidhuber, J. (1997). Long short-term memory. *Neural Comput* 9, 1735–1780.
[64] Nazvanova, A., Ong, M. C., Yin, G. (2023). A data-driven reduced-order model based on long short-term memory neural network for vortex-induced vibrations of a circular cylinder. *Phys. Fluids* 35, 065103.
[65] Bukka, S. R., Gupta, R., Magee, A. R., Jaiman, R. K. (2021). Assessment of unsteady flow predictions using hybrid deep learning based reduced-order models. *Phys. Fluids* 33, 013601.
[66] Gupta, R., Jaiman, R. (2022). Three-dimensional deep learning-based reduced order model for unsteady flow dynamics with variable Reynolds number. *Phys. Fluids* 34, 033612.
[67] Gupta, R., Jaiman, R. (2022). A hybrid partitioned deep learning methodology for moving interface and fluid–structure interaction. *Comput. Fluids* 233, 105239.
[68] Vaswani, A., Shazeer, N., Parmar, N., Uszkoreit, J., Jones, L., Gomez, A. N., Kaiser, Ł., Polosukhin, I. (2017). Attention is all you need. In Proceedings of the 31st International Conference on Neural Information Processing Systems. Long Beach, p 6000–6010.
[69] Yang, S. H., Wang, Y. X., Chu, X. W. (2020). A survey of deep learning techniques for neural machine translation. arXiv preprint arXiv:2002.07526.
[70] Wang, Y. N., Solera-Rico, A., Vila, C. S., Vinuesa, R. (2024). Towards optimal β-variational autoencoders combined with transformers for reduced-order modelling of turbulent flows. *Int. J. Heat Fluid Flow* 105, 109254.
[71] Solera-Rico, A., Sanmiguel Vila, C., Gómez-López, M., Wang, Y. N., Almashjary, A., Dawson, S. T. M., Vinuesa, R. (2024). β-variational autoencoders and transformers for reduced-order modelling of fluid flows. *Nat. Commun* 15, 1361.
[72] Pasta, E., Faedo, N., Mattiazzo, G., Ringwood, J. V. (2023). Towards data-driven and data-based control of wave energy systems: Classification, overview, and critical assessment. *Renew. Sustain. Energy Rev* 188, 113877.
[73] Bernitsas, M. M., Raghavan, K., Ben-Simon, Y., Garcia, E. M. H. (2008). VIVACE (vortex induced vibration aquatic clean energy): A new concept in generation of clean and renewable energy from fluid flow. *J. Offshore Mech. Arct. Eng* 130, 041101.
[74] Semeraro, O., Bagheri, S., Brandt, L., Henningson, D. S. (2011). Feedback control of three-dimensional optimal disturbances using reduced-order models. *J. Fluid Mech* 677, 63–102.
[75] Semeraro, O., Pralits, J. O., Rowley, C. W., Henningson, D. S. (2013). Riccati-less approach for optimal control and estimation: An application to two-dimensional boundary layers. *J. Fluid Mech* 731, 394–417.

[76] Brunton, S. L., Noack, B. R. (2015). Closed-loop turbulence control: Progress and challenges. *Appl. Mech. Rev* 67, 050801.
[77] Rabault, J., Kuchta, M., Jensen, A., Réglade, U., Cerardi, N. (2019). Artificial neural networks trained through deep reinforcement learning discover control strategies for active flow control. *J. Fluid Mech* 865, 281–302.
[78] Tang, H. W., Rabault, J., Kuhnle, A., Wang, Y., Wang, T. G. (2020). Robust active flow control over a range of Reynolds numbers using an artificial neural network trained through deep reinforcement learning. *Phys. Fluids* 32, 053605.
[79] Varela, P., Suárez, P., Alcántara-Ávila, F., Miró, A., Rabault, J., Font, B., García-Cuevas, L. M., Lehmkuhl, O., Vinuesa, R. (2022). Deep reinforcement learning for flow control exploits different physics for increasing Reynolds number regimes. *Actuators* 11, 359.
[80] Ren, F., Zhang, F., Zhu, Y. N., Wang, Z. K., Zhao, F. W. (2024). Enhancing heat transfer from a circular cylinder undergoing vortex induced vibration based on reinforcement learning. *Appl. Therm. Eng* 236, 121919.
[81] Garnier, P., Viquerat, J., Rabault, J., Larcher, A., Kuhnle, A., Hachem, E. (2021). A review on deep reinforcement learning for fluid mechanics. *Comput. Fluids* 225, 104973.
[82] Han, B. Z., Huang, W. X., Xu, C. X. (2022). Deep reinforcement learning for active control of flow over a circular cylinder with rotational oscillations. *Int. J. Heat Fluid Flow* 96, 109008.
[83] Xu, H., Zhang, W., Deng, J., Rabault, J. (2020). Active flow control with rotating cylinders by an artificial neural network trained by deep reinforcement learning. *J. Hydrodyn* 32, 254–258.
[84] Fan, D. X., Yang, L., Wang, Z. C., Triantafyllou, M. S., Karniadakis, G. E. (2020). Reinforcement learning for bluff body active flow control in experiments and simulations. *Proc. Natl. Acad. Sci. USA* 117, 26091–26098.
[85] Li, J. C., Zhang, M. Q. (2022). Reinforcement-learning-based control of confined cylinder wakes with stability analyses. *J. Fluid Mech* 932, A44.
[86] Yousif, M. Z., Kolesova, P., Yang, Y. F., Zhang, M., Yu, L. Q., Rabault, J., Vinuesa, R., Lim, H. C. (2023). Optimizing flow control with deep reinforcement learning: Plasma actuator placement around a square cylinder. *Phys. Fluids* 35, 125101.
[87] Raissi, M., Perdikaris, P., Karniadakis, G. E. (2019). Physics-informed neural networks: A deep learning framework for solving forward and inverse problems involving nonlinear partial differential equations. *J. Comput. Phys* 378, 686–707.
[88] Rao, C. P., Sun, H., Liu, Y. (2020). Physics-informed deep learning for incompressible laminar flows. *Theor. Appl. Mech. Lett* 10, 207–212.
[89] Jin, X. W., Cai, S. Z., Li, H., Karniadakis, G. E. (2021). NSFnets (Navier-Stokes flow nets): Physics-informed neural networks for the incompressible Navier-Stokes equations. *J. Comput. Phys* 426, 109951.
[90] Yan, C., Xu, S. F., Sun, Z. X., Guo, D. L., Ju, S. J., Huang, R. F., Yang, G. W. (2023). Exploring hidden flow structures from sparse data through deep-learning-strengthened proper orthogonal decomposition. *Phys. Fluids* 35, 037119.
[91] Cai, S. Z., Mao, Z. P., Wang, Z. C., Yin, M. L., Karniadakis, G. E. (2021). Physics-informed neural networks (PINNs) for fluid mechanics: A review. *Acta Mech. Sin* 37, 1727–1738.
[92] Xu, S. F., Yan, C., Zhang, G. T., Sun, Z. X., Huang, R. F., Ju, S. J., Guo, D. L., Yang, G. W. (2023). Spatiotemporal parallel physics-informed neural networks: A framework to solve inverse problems in fluid mechanics. *Phys. Fluids* 35, 065141.
[93] Eivazi, H., Wang, Y. N., Vinuesa, R. (2024). Physics-informed deep-learning applications to experimental fluid mechanics. *Meas. Sci. Technol* 35, 075303.
[94] Raissi, M., Wang, Z. C., Triantafyllou, M. S., Karniadakis, G. E. (2019). Deep learning of vortex-induced vibrations. *J. Fluid Mech* 861, 119–137.
[95] Cheng, C., Meng, H., Li, Y. Z., Zhang, G. T. (2021). Deep learning based on PINN for solving 2 DOF vortex induced vibration of cylinder. *Ocean Eng* 240, 109932.
[96] Bai, X. D., Zhang, W. (2022). Machine learning for vortex induced vibration in turbulent flow. *Comput. Fluids* 235, 105266.
[97] Tang, H. S., Liao, Y. Y., Yang, H., Xie, L. Y. (2022). A transfer learning-physics informed neural network (TL-PINN) for vortex-induced vibration. *Ocean Eng* 266, 113101.
[98] Menon, K., Mittal, R. (2020). Dynamic mode decomposition based analysis of flow over a sinusoidally pitching airfoil. *J. Fluids Struct* 94, 102886.
[99] Menon, K., Mittal, R. (2021). Quantitative analysis of the kinematics and induced aerodynamic loading of individual vortices in vortex-dominated flows: A computation and data-driven approach. *J. Comput. Phys* 443, 110515.
[100] Stankiewicz, W., Roszak, R., Morzyński, M. (2013). Arbitrary Lagrangian–Eulerian approach in reduced order modeling of a flow with a moving boundary. *Prog. Flight Phys* 5, 109–124.
[101] Schmid, P. J., Henningson, D. S., Jankowski, D. F. (2002). Stability and transition in shear flows. Applied mathematical sciences, vol. 142. *Appl. Mech. Rev* 55, B57–B59.
[102] Miyanawala, T. P., Jaiman, R. K. (2019). Decomposition of wake dynamics in fluid–structure interaction via low-dimensional models. *J. Fluid Mech* 867, 723–764.
[103] Yao, W., Jaiman, R. K. (2017). Model reduction and mechanism for the vortex-induced vibrations of bluff bodies. *J. Fluid Mech* 827, 357–393.
[104] Tong, W. W., Yang, Y., Wang, S. Z. (2021). Estimating thrust from shedding vortex surfaces in the wake of a flapping plate. *J. Fluid Mech* 920, A10.
[105] Hanrahan, S., Kozul, M., Sandberg, R. D. (2023). Studying turbulent flows with physics-informed neural networks and sparse data. *Int. J. Heat Fluid Flow* 104, 109232.
[106] Patel, Y., Mons, V., Marquet, O., Rigas, G. (2024). Turbulence model augmented physics-informed neural networks for mean-flow reconstruction. *Phys. Rev. Fluids* 9, 034605.
[107] Chuang, P. Y., Barba, L. A. (2023). Predictive limitations of physics-informed neural networks in vortex shedding. arXiv preprint arXiv:2306.00230.